Surface Diffusion and Substrate–Nanowire Adatom Exchange in InAs Nanowire Growth

Shadi A. Dayeh,*,† Edward T. Yu, and Deli Wang

Department of Electrical and Computer Engineering, University of California at San Diego, La Jolla, California 92093-0407

ABSTRACT

We report new fundamental insights into InAs nanowire (NW) nucleation and evolution on InAs (111)B surfaces using organometallic vapor phase epitaxy and present the first experimental demonstration of two distinct NW growth regimes, defined by the direction of substrate–NW adatom exchange, that lead to nonlinear growth rates. We show that the NW elongation rate and morphology in these two growth regimes are governed by the relative difference between the In adatom diffusion lengths on the growth substrate surface and on the NW sidewalls, resulting in strong growth rate dependence on the NW length. These results indicate that surface solid–phase diffusion of In adatoms is a key process in InAs NW growth, which is also supported by diameter-dependent growth rates. These developments enable rational growth of axial and radial NW heterostructures.

Bottom-up assembly of nanoengineered materials holds promise for enabling a variety of advances in electronic and optoelectronic devices, including further device miniaturization with high integration density leading to enhanced performance and versatile functionality. In bottom-up assembly, the active elements of a three-dimensional (3D) device are formed by synthetic means without further structural processing. This is in contrast to the top-down processing technique in which lithography is typically used to define the active portions of a 3D device. Among different materials synthesized through the bottom-up technique such as carbon nanotubes[1] and graphene,[2] semiconductor nanowires (NWs) are currently the most precisely controllable bottom-up assembled nanostructures in several aspects including morphology over large areas, conductivity (semiconducting vs a mixture of both semiconducting and metallic), and doping. Semiconductor NWs enable novel axial[3–5] and radial[6] heterostructure growth, surround-gate field-effect transistor (FET) architectures,[7,8] and efficient band gap engineering via the influence of size[9] and alloy[10] composition on electronic properties. Among different semiconductor NWs, III–V NWs are of great interest for their rich properties for electronic and optoelectronic applications and potential of integration to CMOS offered by the bottom-up method.[11] Optimal control over the morphology, and consequently properties, of NWs together with understanding and identifying the limits within which these morphologies

are attainable is essential for utilizing predictable and reproducible NW devices in future technological applications. Our earlier studies have shown that the growth temperature and the TMIn flow rate are key to control the InAs NW morphology.[12,13] In pursuit of understanding the NW growth evolution and determining the relevant diffusion mechanism during their growth, time-dependent growth studies revealed the growth time as another key controlling parameter for NW morphology control and shed light on several other relevant key processes that are discussed in detail below.

Current approaches in understanding the kinetic and thermodynamic aspects of III–V NW growth rely on analysis of growth rates as a function of diameter and interwire spacing to shed light on whether solid–phase diffusion of reactant adatoms,[14] gas–phase diffusion,[15] or the Gibbs–Thomson effect (reduction of vapor pressure with size) is dominant.[16] Several models that take into account these effects have thus emerged.[17–19] In this work, we pursue a different approach that utilizes time-dependent growth rates at different trimethylindium precursor flows to identify two substrate–NW adatom exchange regimes and confirm the occurrence of solid-phase diffusion of In adatoms on the NW sidewalls, which is also supported by analysis of diameter-dependent NW growth rates. These systematic time-dependent analyses presented here[20] have not been performed in earlier experimental studies but are in strong agreement with theoretical predictions,[21] and the resulting understanding leads to better control over InAs NW growth and sets the limits within which uniform InAs NWs and subsequent hetero-

* Corresponding author, shadi@lanl.gov.
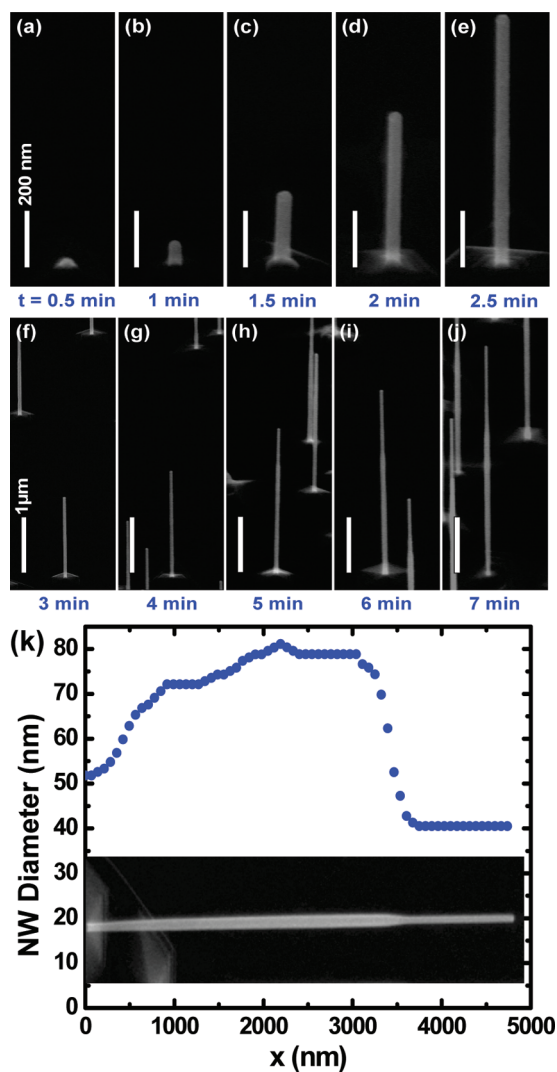† Currently at the Center of Integrated Nanotechnologies, Los Alamos National Laboratory, Los Alamos, NM, 87545.

Figure 1. (a−j) 45° angle view FE-SEM images of InAs NWs grown with 1 μmol/min TMIn flow rate at 500 °C for different growth times. (k) NW diameter profile along the length of an InAs NW grown for 7 min, (FE-SEM image of NW is inset) showing a uniform section near its tip whose length is ∼1 μm.

structure NW morphologies can be obtained through OM-VPE on InAs (111)B surfaces.

Panels a−j of Figure 1 show a 45° angle view of field emission scanning electron microscopy (FE-SEM) images of InAs NWs grown at a constant temperature and TMIn flow rate of 500 °C and 1 μmol/min, respectively, for growth times ranging from 30 s to 7 min. For short growth times (Figure 1a−e), uniform NWs 40 nm in diameter, corresponding to that of the Au nanoparticles, are observed with apparent nonlinear elongation with time. For long growth times (Figure 1f−j), the NW diameter is ∼40 nm close to the NW tip and close to the substrate surface and larger than 40 nm across the major portions of the NW. Variation of the NW diameter across the length of a single NW grown for 7 min is quantified in Figure 1k. The NW length increases linearly with time in Figure 1f−j. In addition, planar growth (i.e., pyramidal structures) at the bottom of the InAs NW increases with time while the NW maintains a uniform diameter as time progresses (Figure 1a−e). This, together
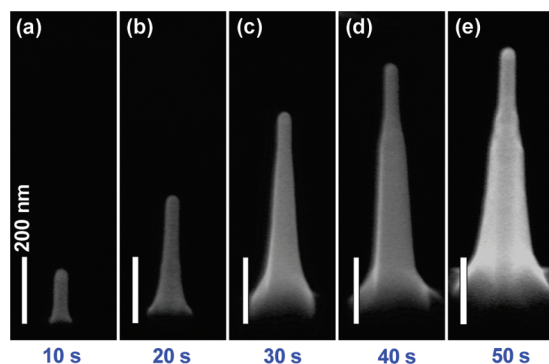

Figure 2. 45° angle view FE-SEM images of InAs NWs grown with 6 μmol/min TMIn flow rate at 500 °C for different growth times.

with the fact that the diameter of the NW base for most NWs is always close to ∼40 nm for all t, indicates that the substrate acts as a material sink for adatoms that adsorb on the NW sidewall within a distance from the substrate comparable to the In adatom surface diffusion length on the NW sidewalls, λ_{NW}, and suggests that the In adatom diffusion length on the substrate surface, λ_{sub}, is much shorter than λ_{NW}.

For a TMIn flow rate of 6 μmol/min, and otherwise similar growth conditions to those used above, the elongation rate and NW morphology are very different from those obtained at 1 μmol/min, as shown in Figure 2a−e. The NWs are tapered, with larger diameter at their bases compared to their tips, for all t, and the NW nucleation occurs at an earlier growth time, where a significant NW length is observed at 10 s (Figure 2a) compared to a slightly shorter NW at 1 min with a TMIn flow rate of 1 μmol/min (Figure 1c). The NW tapering from the base to the tip is indicative of In adatom concentration gradient and associated diffusion from the substrate to the NW. Long growth times at this high TMIn flow rate lead to multiple NW nucleation per single Au NP such that the NW lengths per sample vary significantly.[22] These data reveal a strong substrate−NW interaction for both TMIn flow rates.

Figure 3 shows a plot of InAs NW length as function of time for both TMIn flow rates of 1 and 6 μmol/min. It can be seen clearly from Figure 3 that for a TMIn flow rate of 1 μmol/min, the NW length increases exponentially for short growth time and becomes linear after about 3 min. Since $\lambda_{sub} < \lambda_{NW}$, the collection area of In adatoms is only the NW sidewalls. When the NW length, l, is shorter than λ_{NW}, the collection area of impinging In adatoms on the NW sidewalls ($2\pi r l$ where r as the NW radius) increases continuously with time leading to a superlinear, namely, an exponential increase of the NW length with time. For longer growth times, where $l > \lambda_{NW}$, the collection area for In adatoms remains constant at $2r\pi\lambda_{NW}$ leading to a linear increase of NW length with time. This linear increase in the NW length with time has been frequently observed in III−V NW growth, including InAs NWs grown by chemical beam epitaxy (CBE).[23] The effect of surface diffusion is further manifested in the change of the NW diameter during growth. Figure 1k shows the NW diameter profile along the axis of a long NW grown for 7 min where the NW diameter is larger
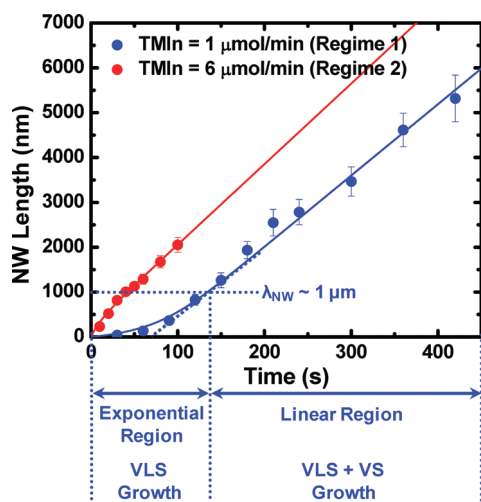
Figure 3. Plot of the NW length as function of time for TMIn flow rates of 1 μmol/min (regime 1) and 6 μmol/min (regime 2). The solid lines are fits for regimes using equation (SE2).

than its counterparts at the NW base and tip. Figure S1a in Supporting Information shows a plot the NW diameter measured at $l/2$ as a function of time indicating that the NW diameter remains constant at ~40 nm in the superlinear growth regime ($l < \lambda_{NW}$) and increases linearly with time in the linear regime ($l > \lambda_{NW}$) due to vapor–solid (VS) or thin film deposition on the NW sidewalls (adatoms cannot make it to the tip anymore and deposit on the NW sidewalls or desorb).

On the other hand, a TMIn flow rate of 6 μmol/min leads to slightly sublinear NW elongation for short growth times, faster than that for a TMIn flow rate of 1 μmol/min, followed by linear elongation as shown in Figure 3. The NW diameter, measured at $l/2$, increases linearly for nearly all t, as shown in Figure S1b in Supporting Information, and uniform NW morphology cannot be attained. The rapid increase in the NW diameter does not permit simple comparison and scaling in the NW lengths obtained for the two TMIn flow rates. Indeed, the increase in the NW volume does not correspond to a 1:1 increase with the TMIn flow rate increase. The ratio of the NW volume with a growth time of 30 s and 6 μmol/min TMIn flow rate to that of 30 and 60 s growth times and 1 μmol/min TMIn flow rate is ~42 and 13, respectively, indicating additional substrate contribution for the larger TMIn flow rate. This, in addition to the trends in the NW morphology and elongation rates implies different substrate–NW adatom exchange in each case of TMIn flow.

The NW elongation rate with time in the context of surface diffusion has been discussed in early studies on growth of whiskers (micrometer or submicrometer diameter wires, which will be referred to as NWs from this point on) even before the vapor–liquid–solid[24] growth mechanism was developed. Dittmar and Neumann were the first to solve the diffusion equation for NW growth[16] and Blakely and Jackson,[25] Ruth and Hirth,[21] and Simmons et al.[26] have solved similar equations with different boundary conditions and approximations. Ruth and Hirth however have considered the substrate–NW adatom exchange and identified regimes in

which the NW elongation varies nonlinearly with time depending on this exchange. The general solution for NW growth rate according to Ruth and Hirth is overviewed in the Supporting Information. A key parameter that identifies the NW growth regime in Ruth and Hirth's model is the term $\beta \propto \lambda_{sub}/\lambda_{NW}$ which indicates the direction and strength of adatom exchange between the substrate and the NW. If $\lambda_{NW} \gg \lambda_{sub}$ and neglecting collection from the NW seed compared to that of the NW sidewalls, the general solution for the NW growth rate (eq SE1) can then be approximated as

$$\frac{dl}{dt} = V_L \tanh\left(\frac{\sqrt{2}l}{\lambda_{NW}}\right) \tag{1}$$

where V_L is the linear growth rate (see Supporting Information), which is the typical elongation rate obtained when not considering the substrate–NW adatom exchange.[16] The solution of eq 1 in the limiting cases of l when compared to λ_{NW} can be obtained as

$$l = \begin{cases} A e^{2^{1/2}V_L t/\lambda_{NW}} & \text{for } l \ll \lambda_{NW} \\ V_L t & \text{for } l \gg \lambda_{NW} \end{cases} \tag{2}$$

These equations precisely portray the experimental trends observed in Figure 3 for the low TMIn flow rate, where exponential NW elongation is obtained for short growth times followed by linear elongation for long growth times. The transition from exponential to linear elongation allows us to extract a value for λ_{NW} of ~1 μm as illustrated in Figure 3. Indeed, the length of the uniform NW section at the NW tip in Figure 1k for long growths is ~1 μm, which is in agreement with λ_{NW} extracted from Figure 3.

On the other hand, when $\lambda_{sub} \sim \lambda_{NW}$ such that $\beta > 1$, In adatom diffusion from the substrate to the NW prevails and the NW elongation proceeds sublinearly for short growth time followed by linear elongation for long growth times according to eq SE2. The experimental data for the two TMIn flow rates was fitted using eq SE2. For the low TMIn flow rate, the curve fit using eq SE2 is obtained for $\beta = 0$ (no substrate–NW adatom exchange is assumed), $V_L = 14$ nm/s, which is determined experimentally from the slope of l vs t in Figure 3 for long growth time, $I \sim 2$ nm/s, and $\lambda_{NW} = 1$ μm, which is in agreement with that obtained from the exponential–linear transition length in Figure 3. For the large TMIn flow rate, the line fit was obtained for $V_L = 16$ nm/s (~17.5 nm/s is extracted experimentally from Figure 3) and $\beta = 2.5$. This simple substitution in eq SE2 resulted in sublinear NW elongation for short growth time followed by linear elongation, which agrees with our experimental observations for high TMIn flow rates with $\beta > 1$ indicating strong substrate contribution to the NW growth.

The validity of solid–phase diffusion to InAs NW growth is further supported by diameter-dependent growths from patterned Au nanoparticles with 2 μm spacing and different disk diameters on InAs (111)B surfaces at growth conditions similar to those used in Figure 1 but in a vertical flow OMVPE system and correspondingly scaled flow rates. For a growth time of 120 s, the NWs with the smallest diameter, 45 nm, grow faster than those with larger diameters of 70 and 90 nm as shown in Figure 4a–c, a trend which is in
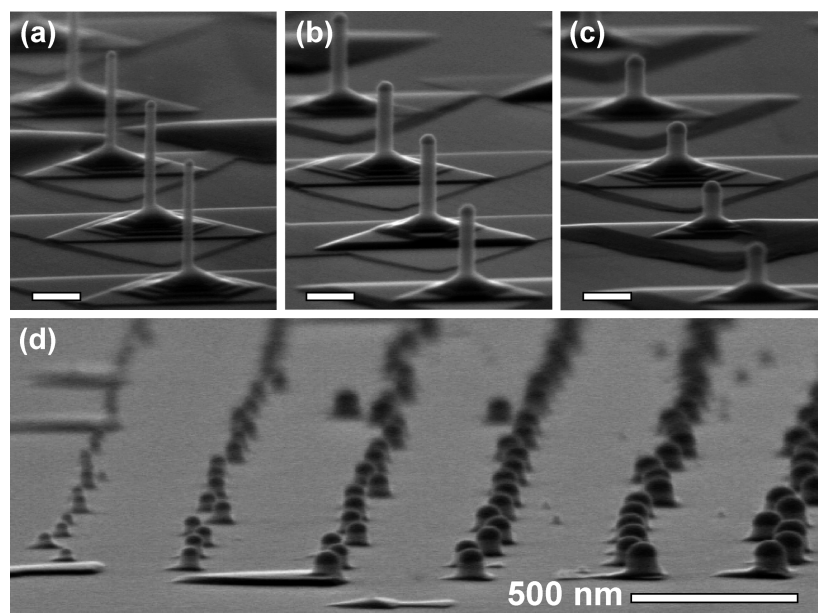
Figure 4. 83° angle view FE-SEM images of InAs NWs grown at predefined locations on the same substrate for 120 s with different diameters (a) 45 nm, (b) 70 nm, and (c) 90 nm. Scale bars are 200 nm. (d) 83° angle view FE-SEM images of InAs NWs grown at predefines locations on the same substrate for 30 s with variable diameters of 45 nm (leftmost column) to 115 nm (rightmost column).

agreement with other studies on InAs NWs.[23] This increase in NW length with smaller diameters suggests that the Gibbs−Thomson effect[16] in a molten Au−In alloy during the InAs NW growth, at least for the range of diameters under consideration here, does not play a significant role. However, growth for a short time, 30 s, reveals that NWs grown from smaller diameter particles nucleate later than those of larger diameter particles as shown in Figure 4d implying that an effect such as the Gibbs−Thomson effect may be relevant during the initial steps of the growth. The time-dependent analysis in this work concerns with NW elongation and morphology postnucleation. Thus, a surface diffusion mechanism is the relevant one in the OMVPE growth of InAs NWs which is consistent with NW diffusion modeling theories discussed earlier.

These results allow us to identify two NW growth regimes dependent on the direction of substrate−NW adatom exchange (Figure 3). In regime 1, minimal to no substrate−NW adatom diffusion occurs and the NW elongation proceeds exponentially via the VLS growth mechanism for $l < \lambda_{NW}$, and linear NW elongation via VLS in addition to radial VS arises for $l > \lambda_{NW}$ as depicted in Figure 3. In regime 2, substrate−NW adatom diffusion prevails with sublinear NW elongation for short growth times and linear elongation for long growth times. NW tapering is persistent in regime 2. Therefore, optimal control over the InAs NW morphology can only be achieved in the VLS portion of regime 1. It is worth mentioning that these InAs NWs exhibit a wurtzite/ zinc blende polymorph crystal structure. The influence of the wurtzite/zinc blende polymorph, NW diameter, and applied fields on the transport properties of these NWs have been discussed in detail elsewhere.[27]

This understanding is of importance for achieving control over radial and axial NW heterostructures. We consider here

the growth of InAs/InP NW heterostructures. Such hetero-structures are important in their axial configuration for performing low-dimensional transport studies[28] or reducing/ eliminating the detrimental effects of surface states[29] in their radial configuration for carrier confinement and high electron mobility applications.[30] Since optimal control over the InAs NW morphology has been demonstrated at low TMIn flow rates (Figure 3, regime 1), the InAs NW segment in any heterostructure combination should be grown in the expo-nential region of regime 1. We consider first the growth of InAs/InP core/shell heterostructure NWs. Such radial het-erostructures have been demonstrated earlier at deposition temperatures of 425 °C/370 °C on InAs (111)B surfaces using CBE,[31] 530 °C/500 °C on SiO_2 surfaces using chemical vapor deposition (CVD),[30] and 420 °C/500 °C on InP (111)B surfaces using OMVPE.[32] High growth temperatures are desired for a crystalline InP shell growth.[30,32] However, this is not possible on InAs (111)B surfaces where the InAs NW cores decomposes even at temperatures similar to their growth temperatures (500 °C) and with AsH_3 overpressure. On InP (111)B surfaces, we did not observe decomposition of the InAs cores, similar to the observation of Li et al.[32] The difference in the InAs core decomposition on InAs (111)B and InP (111)B surfaces may be related to the difference in diffusion lengths and precursor pyrolysis that are surface and orientation dependent.[33] Growth of InAs cores on InP (111)B substrates has similar TMIn flow morphology-dependent trends to those observed on InAs (111)B surfaces. Ideally, after the InAs core growth, the InP shell should be grown without further increase in the NW length. For InAs NWs, we reported a NW growth cessation temperature of ∼510 °C at an input V/III ratio of 60, which we attributed to lack of In supply to the Au nanoparticle (Figure 5).[12] For InP NWs, Dick et al. have reported a cessation temperature
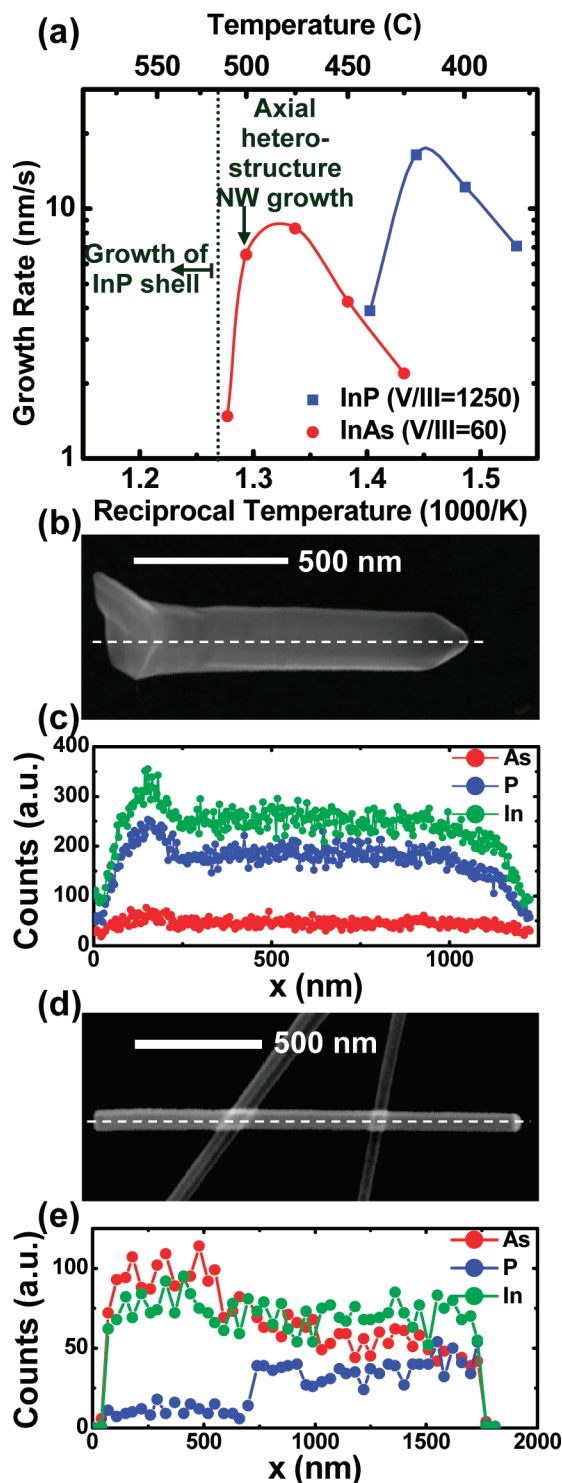
Figure 5. (a) Plot of temperature-dependent growth rate for InAs[12] and InP[35] NWs to aid in growing axial and radial InAs based III−V NW heterostructures with controlled morphology. (b) FE-SEM images of InAs/InP core/shell NW grown for 3−10 min at 500−550 °C, respectively, and (c) EDX spectra along the axis of the same NW shown in (b). (d) FE-SEM images of an InAs/InP axial NW heterostructure grown for 180−120 s at 500 °C and (e) EDX spectra along the axis of the same NW shown in (d).

of ∼450 °C at an input V/III ratio of 1250 (Figure 5).[34] This may indicate that the growth of an InP shell at a V/III ratio of 1250 and a growth temperature of 500 °C directly after the InAs core growth would prevent axial elongation of the

NW and produce a shell coating since the growth temperature of the InP deposition is above that of the cessation temperature of InP NWs (∼450 °C). However, the cessation temperatures shown in Figure 5a are valid only at the NW nucleation stage. Indeed, we have observed that Au nanoparticles that did not nucleate InAs NWs at 500 °C do nucleate InP NWs at 500 °C when AsH_3 is switched to PH_3 whether or not the TMIn flow has been interrupted during the switch over. To cease the axial NW elongation, one would need to stop the In supply and "purge" the Au NP from residual excess In during temperature ramp to that of an InP shell growth. The reduced supersaturation after the temperature ramp-up diminishes the possibility for axial growth and the high growth temperature together with a high input V/III ratio for the InP growth enable InP shell deposition rather than axial elongation. This shell growth region is marked in Figure 5a at temperatures in excess of the cessation temperature of InAs NW growth and is demonstrated in Figure 5b which shows a FE-SEM image of the InAs/InP core/shell on a TEM grid, and Figure 5c which shows an energy dispersive X-ray (EDX) line scan along the NW axis of the In-L, As-L, and P-K lines. Here, the growth of the InAs NW core is performed at 500 °C for 3 min (TMIn flow ∼0.75 μmol/min and AsH_3 flow ∼44.6 μmol/min), after which the temperature is ramped up to 550 °C in AsH_3 flow. The InP shell deposition was performed for 10 min (TMIn flow ∼0.75 μmol/min and PH_3 flow ∼7143 μmol/min, Figure 5b) in an attempt to verify cessation of the axial NW growth and the observation of clear thickening of their diameters under SEM. The large diameter increase from 40 nm for an InAs core to ∼250 nm (Figure 5b) without significant increase in the NW length, which is in agreement with that of Figure 1f, for a long shell deposition time indicates the effectiveness of the core/shell growth method outlined above.

Material requirements and growth conditions for axial heterostructure NW growth are different from those of radial heterostructures[35,36] and are more forgiving in the case of axial InAs/InP heterostructure NWs than the radial ones. We were able to grow InAs/InP axial NW heterostructures on InAs (111)B and InP (111)B substrates, both sections at 500 °C. For this, InAs NWs were first grown for 180 s on an InP (111)B substrate at conditions specified above (Figure 5d), followed by 15 s purge in AsH_3 and 15 s purge in PH_3. The InP section was grown after the InAs section for 120 s. The TMIn, AsH_3, and PH_3 flow rates were ∼1, 44.6, and 7143 μmol/min, respectively. Figure 5d shows a FE-SEM image of the InAs/InP axial NW heterostructure where the total NW length is longer than that in Figure 1f. We found that InP in general has higher nucleation efficiency (could be easily nucleated from In droplets as demonstrated by Novotny and Yu)[37] and higher growth rate (at the same TMIn flow rates) when compared to InAs NWs. Figure 5e shows an EDX line scan along the length of the axial heterostructure NW. In both cases of heterostructure NW growth, we have observed persistent As-L line signal even when the AsH_3 flow has been terminated or purged out indicating either a memory effect from the growth tube or insufficient purge

time. However, morphology control over radial and axial heterostructure NWs in the two growth regimes indicated in Figure 5a is clearly demonstrated.

In conclusion, the first experimental distinction between two NW growth regimes defined by the direction of substrate−NW adatom exchange is demonstrated. Low TMIn flow rates are used to minimize the substrate contribution and obtain uniform InAs NWs whose elongation proceeds exponential for $l < \lambda_{NW}$ and linear for $l > \lambda_{NW}$. The transition between these two elongation rates allowed us to extract a $\lambda_{NW} \sim 1~\mu$m, which is in excellent agreement with the fittings of the experimental data with Ruth and Hirth's model, and with the uniform NW section near the tip of long NWs. High TMIn flow rates result in substrate−NW adatom diffusion and persistent tapering in the NWs with sublinear NW elongation for short growth times and linear elongation for long growth times. This understanding allows us to obtain optimal control over the InAs NW and related NW heterostructure morphologies and sets the limit (within one diffusion length) over which this control is achievable.

Supporting Information Available: Plots of the NW diameter increase with time, as well as an overview of Ruth and Hirth's NW−substrate adatom exchange model. This material is available free of charge via the Internet at http://pubs.acs.org.

References

(1) Iijima, S. *Nature* **1991**, *354*, 56.
(2) Oshima, C.; Nagashima, A. *J. Phys.: Condens. Matter* **1997**, *9*, 1.
(3) Wu, Y.; Fan, R.; Yang, P. *Nano Lett.* **2002**, *2*, 83.
(4) Björk, M. T.; Ohlsson, B. J.; Sass, T.; Persson, A. I.; Thelander, C.; Magnusson, M. H.; Deppert, K.; Wallenberg, L. R.; Samulason, L. *Nano Lett.* **2002**, *2*, 87.
(5) Gudiksen, M. S.; Lauhon, L. J.; Wang, J.; Smith, D. C.; Lieber, C. M. *Nature* **2002**, *415*, 617.
(6) Lauhon, L. J.; Gudiksen, M. S.; Wang, D.; Lieber, C. M. *Nature* **2002**, *420*, 57.
(7) Ng, H. T.; Han, J.; Yamada, T.; Nguyen, P.; Chen, Y. P.; Meyyappan, M. *Nano Lett.* **2004**, *4*, 1247.
(8) Bryllart, T.; Wernersson, L.-E.; Fröberg, L. E.; Samuelson, L. *IEEE Electron Device Lett.* **2006**, *27*, 323.
(9) Gudiksen, M. S.; Wang, J.; Lieber, C. M. *J. Phys. Chem. B* **2002**, *106*, 4036.
(10) Trägårdh, J.; Persson, A. I.; Wagner, J. B.; Hessman, D.; Samuelson, L. *J. Appl. Phys.* **2007**, *101*, 123701.
(11) (a) Dayeh, S. A.; Chen, P.; Jing, Y.; Yu, E. T.; Lau, S. S.; Wang, D. *Appl. Phys. Lett.* **2008**, *93*, 203109. (b) Martensson, T.; Svensson, C. P. T.; Wacaser, B. A.; Larsson, M. W.; Seifert, W.; Deppert, K.; Gustafsson, A.; Wallenberg, L. R.; Samuelson, L. *Nano Lett.* **2004**, *4*, 1987. (c) Bakkers, E. P. A. M.; Borgstrom, M. T.; Verheijen, M. A. *MRS Bull.* **2007**, *32*, 117.
(12) Dayeh, S. A.; Yu, E. T.; Wang, D. *Nano Lett.* **2007**, *7*, 2486.
(13) Dayeh, S. A.; Yu, E. T.; Wang, D. *J. Phys. Chem. C* **2007**, *111*, 13331.
(14) Jensen, L. E.; Björk, M. T.; Sören, J.; Persson, A. I.; Ohlsson, B. J.; Samuelson, L. *Nano Lett.* **2004**, *4*, 1961.
(15) Borgström, M. T.; Immink, G.; Ketelaars, B.; Algra, R.; Bakkers, E. P. A. M. *Nat. Nanotechnol.* **2007**, *2*, 541.
(16) Givargizov, E. I *Highly Anisotropic Crystals*; Springer: Berlin, 1987; pp 100−103.
(17) Johansson, J.; Svensson, C. P. T.; Martensson, T.; Samuelson, L.; Seifert, W. *J. Phys. Chem. B* **2005**, *109*, 13567.
(18) Dubrovskii, V. G.; Cirlin, G. E.; Soshnikov, I. P.; Tonkikh, A. A.; Sibirev, N. V.; Samsonenko, Y. B.; Ustinov, V. M. *Phys. Rev. B* **2005**, *71*, 205325.
(19) Chen, Z.; Cao, C. *Appl. Phys. Lett.* **2006**, *88*, 143118.
(20) The growth experiments were performed in a horizontal OMVPE growth tube using trimethylindium (TMIn) and arsine (AsH₃) precursors in 1.2 L/min H_2 carrier gas and at a chamber pressure of 100 Torr. Forty nanometer diameter Au nanoparticles were dispersed at a density of ∼0.4 μm^{-2} on InAs (111)B substrates precoated with poly-L-lysine, followed by UV ozone cleaning at 100 °C for 5 min. AsH₃ flow was maintained in the chamber throughout the entire growth process including temperature ramp up and cool down, while TMIn was introduced after reaching the desired growth temperature and maintained for the duration of the growth. For patterned growths, e-beam lithography (Joel 6400 operated at 35 keV) was employed in a double-layer MMA/PMMA resist with variable dot sizes. Twenty five nanometer Au was evaporated and lifted off in acetone at room temperature and was consequently used in the growth. The NW morphology was characterized using an FEI XL 30 field emission scanning electron microscope (FE-ESEM) operating at an acceleration voltage of 30 kV. Dimensions and statistical distributions were determined in each case by measuring the sizes of 15 NWs at the highest achieved magnifications.
(21) Ruth, V.; Hirth, J. P. *J. Chem. Phys.* **1964**, *41*, 3139.
(22) Dayeh, S. A.; Yu, E. T.; Wang, D. *Small* **2007**, *3*, 1683.
(23) Jensen, L. E.; Björk, M. T.; Jeppesen, S.; Persson, A. I.; Ohlsson, B. J.; Samuelson, L. *Nano Lett.* **2004**, *4*, 1961.
(24) Wagner, R. S.; Ellis, W. C *Appl. Phys. Lett.* **1964**, *4*, 89–90.
(25) Blakely, J. M.; Jackson, K. A. *J. Chem. Phys.* **1962**, *37*, 428.
(26) Simmons, J. A.; Parker, R. L.; Howard, R. E. *J. Appl. Phys.* **1964**, *35*, 2271.
(27) (a) Dayeh, S. A.; Susac, D.; Kavanagh, K. L.; Yu. E. T.; Wang, D. *Adv. Func. Mater.* **2008**, DOI:10.1002/adfm.200801307. (b) Dayeh, S. A.; Yu, E. T.; Wang, D. *Small* **2008**, *5*, 77. (c) Dayeh, S. A.; Susac, D.; Kavanagh, K. L.; Yu, E. T.; Wang, D. *Nano Lett.* **2008**, *8*, 3114.
(28) Björk, M. T.; Ohlsson, B. J.; Thelander, C.; Persson, A. I.; Deppert, K.; Wallenberg, L. R.; Samuelson, L. *Appl. Phys. Lett.* **2002**, *81*, 4458.
(29) (a) Dayeh, S. A.; Soci, C.; Yu, E. T.; Wang, D. *J. Vac. Sci. Technol., B* **2007**, *25*, 11432. (b) Dayeh, S. A.; Soci, C.; Yu, E. T.; Wang, D. *Appl. Phys. Lett.* **2007**, *90*, 233118.
(30) Jiang, X.; Xiong, Q.; Nam, S.; Qian, F.; Li, Y.; Lieber, C. M. *Nano Lett.* **2007**, *7*, 3214.
(31) Zanolli, Z.; Fröberg, L. E.; Björk, M. T.; Pistol, M.-E.; Samuelson, L. *Thin Film Solids* **2006**, *515*, 793.
(32) Li, H.-Y.; Wunnicke, O.; Borgström, M. T.; Immink, W. G. G.; Van Weert, M. H. M.; Verheijen, M. A.; Bakkers, E. P. A. M. *Nano Lett.* **2007**, *7*, 1144.
(33) Reep, D. H.; Ghandi, S. K. *J. Electrochem. Soc.* **1983**, *130*, 675.
(34) Dick, K. A.; Deppert, K.; Karlsson, L. S.; Wallenberg, L. R.; Samuelson, L.; Seifert, W. *Adv. Funct. Mater.* **2005**, *15*, 1603.
(35) Dick, K. A.; Kodambaka, S.; Reuter, M. C.; Deppert, K.; Samuelson, L.; Seifert, W.; Wallenberg, L. R.; Ross, F. M. *Nano Lett.* **2007**, *7*, 1817.
(36) Paladugu, M.; Zou, J.; Guo, Y.-N.; Auchterlonie, G. J.; Joyce, H. J.; Gao, Q.; Tan, H. H.; Jagadish, C.; Kim, Y. Y. *Small* **2007**, *3*, 1873.
(37) Novotny, C. J.; Yu, P. K. L. *Appl. Phys. Lett.* **2005**, *87*, 203111.

NL900191W